Steinkamp's Toy Can Hop 100 Times But Can't Stand Up

Gregg Stiesberg
Department of Physics,
Cornell University,
Ithaca, NY 14850
e-mail: grs26@cornell.edu

Tim van Oijen
Civil Engineering and Geosciences,
Delft University of Technology,
Delft 2600 AA, The Netherlands
e-mail: T.P.vanOijen@tudelft.nl

Andy Ruina[1]
Department of Mechanical Engineering,
Cornell University,
Ithaca, NY 14850
e-mail: ruina@cornell.edu

We have experimented with and simulated Steinkamp's passive-dynamic hopper. This hopper cannot stand up (it is statically unstable), yet it can hop the length of a 5 m 0.079 rad sloped ramp, with $n \approx 100$ hops. Because, for an unstable periodic motion, a perturbation Δx_0 grows exponentially with the number of steps ($\Delta x_n \approx \Delta x_0 \times \lambda^n$), where λ is the system eigenvalue with largest magnitude, one expects that if $\lambda > 1$ that the amplification after 100 steps, λ^{100}, would be large enough to cause robot failure. So, the experiments seem to indicate that the largest eigenvalue magnitude of the linearized return map is less than one, and the hopper is dynamically stable. However, two independent simulations show more subtlety. Both simulations correctly predict the period of the basic motion, the kinematic details, and the existence of the experimentally observed period ~11 solutions. However, both simulations also predict that the hopper is slightly unstable ($|\lambda|_{max} > 1$). This theoretically predicted instability superficially contradicts the experimental observation of 100 hops. Nor do the simulations suggest a stable attractor near the periodic motion. Instead, the conflict between the linearized stability analysis and the experiments seems to be resolved by the details of the launch: a simulation of the hand-holding during launch suggests that experienced launchers use the stability of the loosely held hopper to find a motion that is almost on the barely unstable limit cycle of the free device. [DOI: 10.1115/1.4035337]

1 Introduction

Toy maker and inventor Peter Steinkamp, who earlier made some interesting passive-dynamic devices, was challenged to make a passive device that cannot stand up but can hop down a ramp. The preceding paper in this journal describes his result [1]. The goal was to make a hopping robot analogous to the Tinkertoy walking device [2]. The Tinkertoy walker is a statically unstable toy that can stably walk down a ramp. There are few other known statically unstable, yet dynamically stable, devices that use no gyroscopic stabilization from spinning parts (e.g., a top, a rolling hoop, and a conventional bicycle depend on spinning parts). Two dynamically stable yet statically unstable devices without spinning parts are the gyro-free bike that self-balances [3] and the dynamically stable skateboard with rigid rider [4]. Through examples such as these, one hopes to learn about the mechanisms of passive stability of such nonholonomic systems. (Nonholonomic systems have an accessible configuration space that has higher dimension than the instantaneously accessible velocity space, for example, systems with 3D rolling, ideal-skate contact, or with intermittent contact.)

More specifically, one wonders about the role of simple passive mechanics in the stability of real and synthetic legged locomotion. The fruit of Steinkamp's systematic and inspired tinkering toward this end, the Steinkamp hopper [1], is the subject of the analysis in this paper.

We contrast these essentially dynamic devices with mechanisms that are dynamically stable near a statically stable equilibrium (like a damped pendulum or damped spring–mass system). In the neighborhood of a potential energy minimum, a damped dynamical device's energy decays toward the bottom of a potential well. That is, total system energy is then a monotonically decreasing Lyapunov function. Because of their potential energy minima, these systems have dynamic stability because of their static stability. In contrast, mechanical systems which are only stable near a state in motion (e.g., a spinning top or a bicycle moving in a straight line), rather than near an equilibrium point, or which have stable limit cycles (e.g., passive-dynamic walking devices), have at least one state variable which increases linearly in time (e.g., the angle of rotation or position on the plane). These systems cannot attribute their stability to that statics concept. Hence, their stability is essentially dynamic.

Statically unstable, yet dynamically stable, systems often have stability dependent on the contributions of gyroscopic terms or nonholonomic contact constraints [5]. Our interest here is in a system whose (presumed) stability is dependent on nonholonomic contact of an intermittent type [5] rather than gyroscopic terms. Independent of engineering or scientific goals, and as for tops, gyroscopes, rolling hoops, and bicycles from past times, models and devices that balance because of motion are intrinsically engaging. With the present research, we aim to better understand one such physical device with the following apparently unique combination of features: it seems to hop stably without tethers; it is statically unstable (the motion of interest is near a configuration which maximizes potential energy with respect to fore-aft tipping); and it has no gyroscopic stabilization nor electronic control.

1.1 Comment on Categorization of Systems.

We loosely categorize the Steinkamp hopper as *passive* and *uncontrolled*. However, within commonly accepted definitions, neither of these designations is precise.

The system is *passive* in that it is made of parts that have no energy sources, and the only external work on the system is from a conservative force (gravity). But the system is not passive in that the gravity force does not have bounded potential energy. So, for example, unlike a damped pendulum, the system's stability does not follow from its passivity.

The system is *uncontrolled* in that there is no consciously designed disjoint electrical control apparatus nor is there such a disjoint mechanical control apparatus. In control theory, the "plant" (the machine) is typically considered disjoint from the "control system." But given a system, engineered or natural, there is no accepted way to precisely delineate what is the plant and what is the control system. It is one big system. Consider the Watt–Maxwell flyball centrifugal regulator. In the engineer's mind, the spinning flyball is a control system. However, looking

[1]Corresponding author.

Manuscript received September 8, 2016; final manuscript received November 8, 2016; published online January 13, 2017. Assoc. Editor: James Schmiedeler.

at the steam-engine as a whole one can choose to see a single passive system, including the flyball mechanism as part of the system. And because electronics also obey the laws of physics, a computer-controlled system is, in some sense, also an uncontrolled system.

Even though the delineations are, as described above, not precise, we make the nonprecise designation that the Steinkamp hopper is passive and uncontrolled in that it is relatively simple, is not designed using control concepts, and has no irreversible power sources. That is, the Steinkamp hopper has only a small number of internal degrees-of-freedom, no electronic components, no mechanical parts explicitly and consciously designed for regulation, and positive mechanical power input coming only from gravity.

1.2 Background on Stability of Hopping and Running Devices. As most famously demonstrated by Marc Raibert and coworkers hoppers in 2D (e.g., see Ref. [6]) and 3D (e.g., see Ref. [7]), powered and *controlled* hopping can be balanced by appropriate controlled foot placement. On the other hand, walking devices can have passive stability with no tethers nor electronic control (e.g., see Refs. [8] and [9]). Passive-dynamic running has been much less explored and arguably (see below) never demonstrated with a physical device. If balance is not a concern, as for 1D vertical hopping in which the only stability concern is regularity of hop height, open-loop actuated one-dimensional hopping simulations and devices have been shown to have stable periodic motions [10,11]. Note that the open-loop control is a slight (also not precisely delineated) generalization of passive dynamics. In one dimension, even with collisional dissipation, passive (no motors and no electronic sensors) hopping can exhibit "one-way" stability [12] toward special nondissipative modes.

To the best of our knowledge, all the two- or three-dimensional hopping or running simulations and devices in the literature have one or more of these features:

(1) *Unstable*: The springy leg offset mass (SLOM) hoppers have distinctly *unstable* passive hopping motions, as shown by simulations of Seth et al. [13]. A passive running device studied by Owaki et al. [14] seems almost stable; when launched by hand it often takes 11–15 steps, but at most 36 steps, before falling on an inclined treadmill.

(2) *Feedback stabilized*: Following Raibert et al. [6,7], and others from Raibert's lab, there have been many physical and simulated demonstrations of actively stabilized hopping or running. Ahmadi and Buehler [15] implemented a simulation model similar to a springy leg, or spring loaded, inverted pendulum (SLIP) with the addition of a torsional spring coupling the body and leg; passive motions are found to be unstable but are stabilized by a feedback controller. In the SLOM (above) simulation of Sayyad et al. [16], actuation to recover energy losses is accomplished by a precompressed linear leg that is triggered by sensing impact; these motions with minimal feedback are unstable but easily stabilized by adding further feedback control using the angle of the body with respect to the floor to modify the leg precompression. The simulations of Geyer et al. [17] and Ghigliazza et al. [18] use minimal feedback control, controlling the leg angle with respect to the floor in flight, thus controlling the leg angle at impact; the simulation of Owaki and Ishiguro [19] controls both the leg angle just before impact and the speed of the forward foot parallel to the leg just after impact. M'Closkey and Burdick [20] studied simplified Raibert-like models with feedback control and found stable motions. The simulations of Hyon and Emura [21] control leg stiffness and the time of leg touchdown to achieve stable motions. Zeglin and Brown [22,23] used discrete feedback control to stabilize an energy efficient 2D bow-legged hopper by specifying the leg angle at touch-down and change in kinetic energy at push-off.

(3) *Simulation only*: Four simulation studies, not complemented by stable physical devices, show passive (or at least open loop) dynamic stability. McGeer's 2D simulations show asymptotically stable passive running [24] for a model that has some internal damping. Cotton's 2D runner inspired by an Ostrich [25] uses open-loop control and nonlinear springs to achieve robust running at speeds as high as 34 kph. The simulations of Mombaur et al. [26] show stability via implementation of optimized open-loop controls. The Owaki et al. [27] simulations show dynamic stability, although their related physical device seems not quite stable (see above).

(4) *Statically stable*: It is most clear that a device has stability essentially dependent on dynamics if the device has no standing static configuration. We could thus exclude McGeer's passive running simulations [24]; the model has two legs and thus a statically stable configuration when the legs are splayed. Similarly, the (almost stable, see above) physical device of Owaki et al. [14] also has two legs and probably has a stable standing posture. But, unlike the case for walkers, this splayed-leg-static-stability exclusion is not so relevant for the runners, as the stable double-stance splayed-leg configuration is never visited in the dynamic running motions. Thus, as opposed to the case for walkers, the existence of a statically stable configuration for bipedal runners is only a somewhat technical defect.
In contrast, the dynamically stable hopping device of Paul et al. [28] has four springy contact points defining a large rectangle, indicating a static stability on which the dynamic stability is likely dependent.

(5) *Gyrostabilization*: While we do not know of any gyrostabilized passive hopping or running robot, there is no doubt that such could be built (Mason Peck—private communication), but it would fall outside the range of the nongyroscopic devices described here.

Thus, there remains the challenge of physically demonstrating a passive hopping or running device that is statically unstable, does not depend on fast-spinning parts, yet is dynamically stable while hopping or running. This was the challenge which Steinkamp took up.

2 The Steinkamp Hopper

After an iterative development, starting with simpler passive toys and then moving on to hopping-like devices Steinkamp built a hopper [1] that, although planar in concept, hops without support in 3D (Fig. 1). Pivotally, Steinkamp's hopper has a small rounded foot with radius much smaller than the center-of-mass (COM) height, hence it is statically unstable. If one attempts to statically balance it and then let go, it falls, like a meter-stick on end, within a second or so. Steinkamp's hopper consists of a more-or-less rigid body and tail (403 g) connected by a leaf spring to a light more-or-less rigid leg (12 g). The body is composed of welded channel aluminum segments, including several weights that are more-or-less easily adjusted, and a vertical carbon-fiber-tube tail.

The weight on the top middle (Figs. 2(*a*) and 1(*b*)) can be slid and tightened to adjust the device's overall center-of-mass (COM) position which is at a height of ≈18 cm. The leg assembly is composed of two legs, each a carbon fiber tube with a round rubber foot of radius ≈1.6 cm. At their tops, the legs, about 2 cm apart, are attached to each other and the leaf spring with a small block of wood (Fig. 1(*c*)). The leaf spring consists of two side-by-side strips of spring steel. The device has a high, slightly flexible tail. The hopper is launched by initially guiding it down a flat, sloped ramp (≈0.079 rad ≈4.5 deg) and then releasing. All of the details above came from Steinkamp's use of intuition and experiments to progressively improve stability. The end result of that evolution is the device we describe here and best understood by the study of the paper by Steinkamp [1] and his associated videos [29].

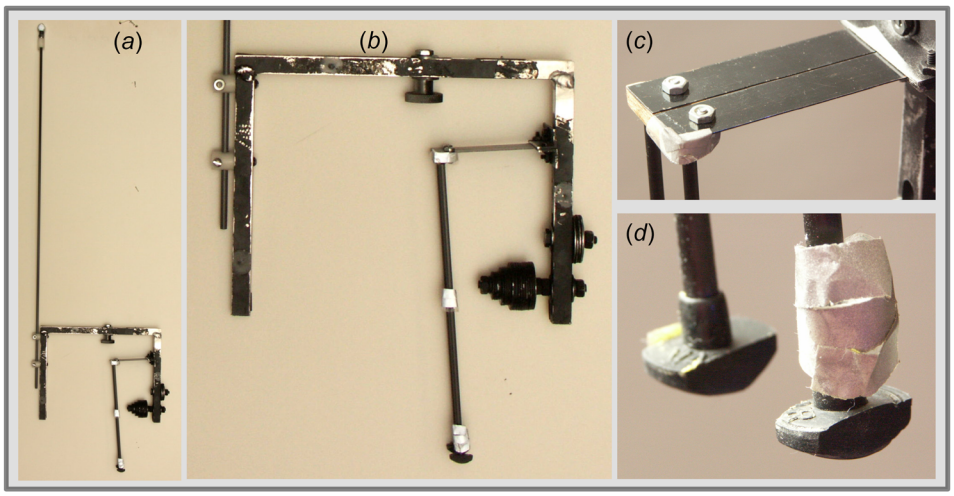

Fig. 1 The Steinkamp hopper: (*a*) the entire device, (*b*) close up of body (compare with Fig. 2(*a*)), (*c*) the leaf spring, and (*d*) the feet (with motion-capture reflective marker tape on one). For more details, see Ref. [1].

The motion of the hopper is vaguely like that of a Kangaroo (see Fig. 3, and Supplementary Videos, which are available under the Supplemental Materials tab for this paper on the ASME Digital Collection). The device hops down a 0.079 rad (≈4.5 deg) slope which was chosen to be similar to the slope found empirically by Steinkamp. It makes about 11 hops per second (period ≈90 ms) at an average forward speed of about 0.5 m/s. The stance phase lasts about 25 ms and swing phase lasts about 65 ms. Starting from the beginning of flight, as the hopper enters the flight phase, the foot accelerates forward and the leg rotates forward about 0.4 rad. (In Fig. 3(*c*), the leg appears to collide with the body, but does not, in either experiments or simulations.) The leg then accelerates backward, giving the foot a backward velocity, relative to the body and also backward relative to the ground, as the foot collides with the ramp. This collision starts the stance phase. In stance, the leg goes up relative to the body, then rotates, and then goes down relative to the body, leading to takeoff. This sequence is one hop (one cycle and one period).

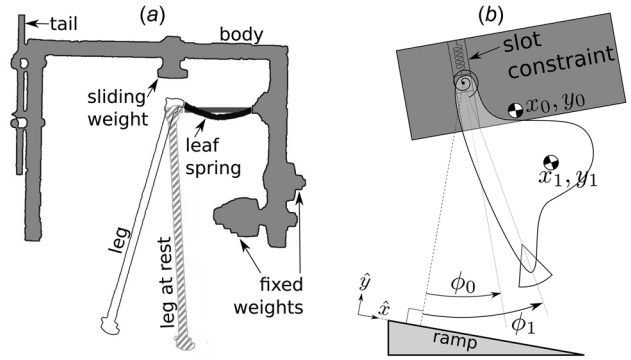

Fig. 2 Schematic of the simulation model. (*a*) The rigid body (gray) and the rigid leg (dark outline with white fill) are connected by a leaf spring (black). The "leg at rest" configuration (striped fill) corresponds to the leg configuration shown in Fig. 1(*b*). The leaf spring allows displacement normal to its length and also rotation (the rotation is never so large as to cause leg collision with the counterweights on the body). The net effect is allowance of leg rotation (leg swing) about the nominal hip and of leg axial motion (body bounce). Horizontal motion of the leg, relative to the body, at the nominal hip, is effectively constrained to zero by the extension stiffness of the leaf spring. (*b*) In the 2D modeling, the body and leg each have two position coordinates and an angle. The constraint from leaf-spring's inextensibility is modeled using a pin in a slot. In one of our simulation models, the slot is in the body (shown), and in the other, the slot is in the leg. The leaf spring is modeled as a coupled torsion–extension viscoelastic spring in which torque and force both depend on displacement and rotation, with the elastic part determined by classical beam theory.

A practiced human can repeatedly launch the hopper on a journey of about 100 hops down the full length of our 5 m ramp in about 9 s. As already emphasized, this device has a small foot and a high center-of-mass. Thus, its (surprising) ability to hop the length of the ramp must be an essentially dynamic phenomenon.

Research question. Our goal was to better understand the nature of the stability of this device. We pursued this by motion-capture observations, modeling, and simulation. We hoped to discover the key features that make the observed repeated hopping possible.

Although the device works in three dimensions, the motion is nearly planar and we have only aimed for a 2D (sagittal plane, longitudinal, side-view, and fore-aft) analysis. Even with the laterally (side-to-side) separated feet, in a dynamics context we cannot claim triviality of the steering stability that is present and visible in the experiments, nor the evident stability against sideways falling. Nonetheless, we do not study these 3D features of the device here. The 2D dynamics is our focus.

2.1 Experiments. With Steinkamp's help, we collected motion-capture data using a Vicon infrared camera system. We put reflective markers on various points on the hopper to get position versus time data. We collected data for 77 separate trials that resulted in sustained hopping. Of these 77 data sets, 37 of them show at least 3 m of hopping and 16 of these show more than 4 m of hopping. (There are about 20–25 hops per meter.) The position data, with a consistency of about 1–2 mm and an accuracy of about 3 mm, were filtered and numerically differentiated to extract velocities. Some observations are:

(1) *Launch*: It takes some practice to launch reliably. For beginners, the result is often a few hops and then a fall to front or back.

A successful launch is shown at minute 3:02 of the video "Steinkamp Hopper at Cornell" (see video under the Supplemental Data tab for this paper on the ASME digital collection). The device is oriented to go down the ramp, such that the rear of the horizontal body bar is about 3 cm lower than the front, matching the orientation of nominally stable hopping. The launcher stands to the left of the device,

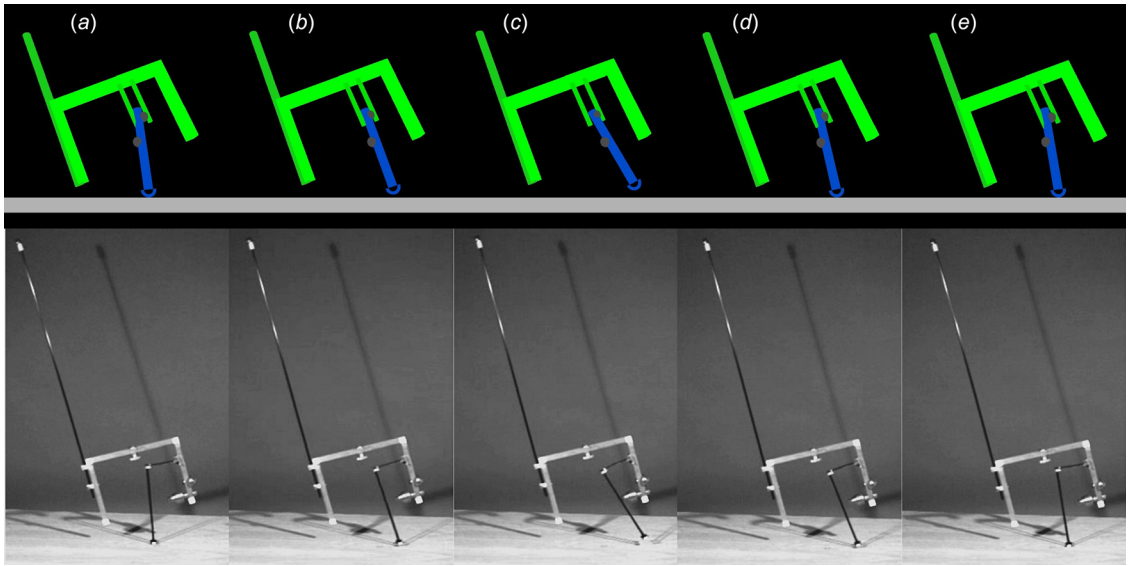

Fig. 3 One step of hopper motion. The photo is rotated slightly counterclockwise so that the actual slope, down and to the right, appears as horizontal. The motion is from left to right. The natural orientation of the device, while hopping, is rotated ≈10 deg counterclockwise compared to schematic views in Figs. 1(*b*) and 2(*a*). One hop cycle is shown from simulation (discussed at length below) and from slow motion video. (*a*) At liftoff, the backward force on the foot from the ground is relieved, and the body moves upward; (*b*) as the device moves forward and upward, the leg swings forward; (*c*) near the apex of the hop, the leg movement reverses direction (the leg comes close to, but does not collide with the body); (*d*) while dropping in height, just before the foot collides with the floor, the leg is still swinging backward relative to both body and ground (swing leg retraction [30,31]); and (*e*) in contact with the floor, the leg compresses and pushes the body upward again (video stills courtesy of Steinkamp).

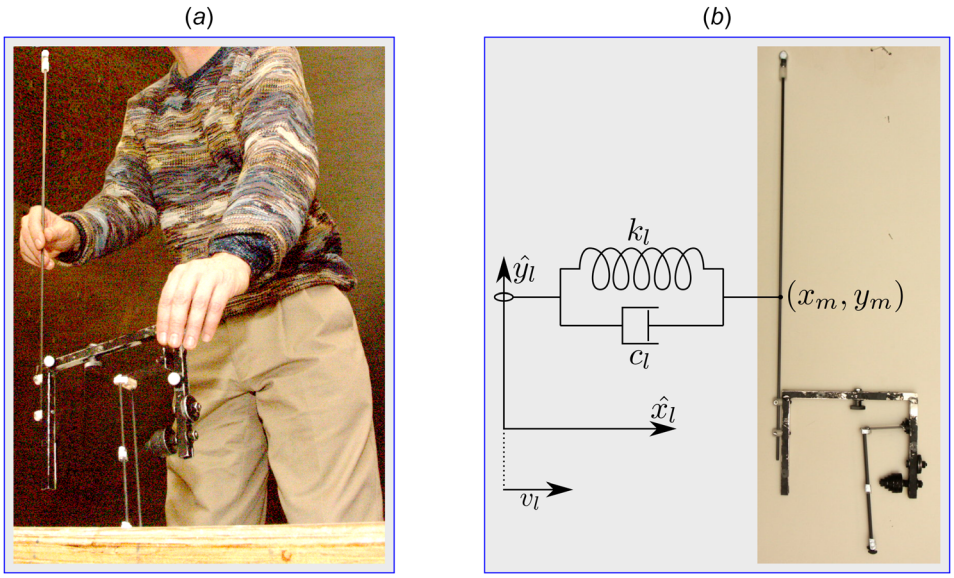

Fig. 4 Hand-held launch. (*a*) The tail of the device is held gently above the back of the body (Steinkamp's right hand) for the first ≈10 to 15 hops, then released. See text for details (photo background darkened for clarity, the slope is down and to the right but appears as nearly level due to camera perspective); (*b*) shock-absorber-attached model of launch. In simulations of launch, we model the right-hand holding as a shock absorber attached between the point (x_m, y_m) on the tail, and where the hand is an imaginary reference point moving at a constant launch speed v_l.

holding it initially with both hands. The left hand is at the top front corner and the right hand at the tail, approximately 20 cm above the body (Fig. 4(*a*)). The device is then, in the air, moved (swung and swept) forward and downward until the leg makes contact with the ramp, exciting successive foot bounces and leg swings. If this leg scraping and bouncing are sufficiently periodic, then the front hand is released, and the robot is only held loosely by the tail with the right hand. If and when there is satisfactorily periodic leg excitement, the right hand is moved along with the hopping robot, controlling its pitch (fore-aft tottering) and forward speed. If and when the fore-aft tottering is sufficiently

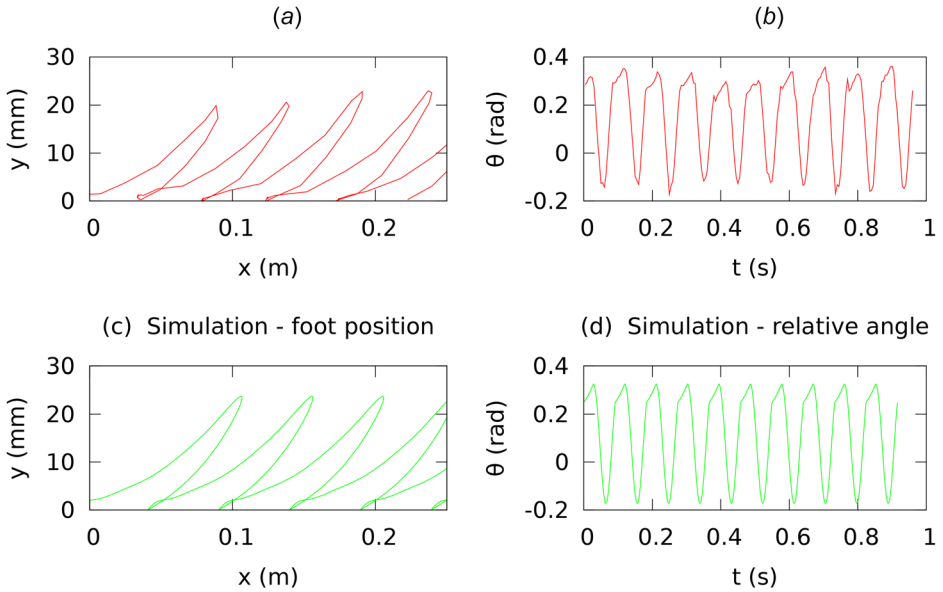

Fig. 5 Foot position versus distance, measured and simulated. (*a*) A magnified view of the path of a point on the foot from motion-capture data and (*c*) from simulation. Note the small loop made by the foot as it pivots and lifts off. The vertical scale is exaggerated to enhance the details of the motion. Relative angle versus time, measured and simulated. (*b*) The relative angle between the body and leg from motion-capture data and (*d*) from simulation.

minimal and the speed is satisfactory, usually after 10–15 hand-assisted hops, the rear hand is withdrawn from the tail. Just before hand release, the force of the hand on the hopper seems small. The device then often hops the remaining length of the ramp (approximately 4 m, about 100 hops).

(2) *Elasticity of the tail*: Steinkamp's motivation for adding the tail was to inhibit body pitch without adding a lot of mass. As constructed by Steinkamp, the tail is elastic and wobbles during the hopping. Is that wobble essential? We tied a diagonal string from near the top of the tail to the main body, almost eliminating the tail vibrations. This reduction of tail motion had no detectable effect on any aspect of the hopper's overall motion. Thus, the function of the tail seems only to be to increase the body's polar moment-of-inertia (that is, the tail does not add a useful independent degree-of-freedom). An unintended, and possibly key, benefit of the tail is to serve as a hand-hold in launch.

(3) *Details of the motion*: The overall motion is shown in Fig. 3 and (under the Supplemental Data tab for this paper on the ASME digital collection). The trajectory of the foot, and of the relative angle of the body and leg, is shown in Fig. 5.

(4) *Approximately period* ∼11 *motion*: Figure 6(*a*) shows the foot height over about 30 cycles from motion-capture data. The amplitude varies in a periodic manner, with a period of about, but not precisely, 11 hops, ranging from about nine hops/s up to about 11 hops/s. For the rest of this paper, we refer to this as the "period ∼11 motion." This amplitude modulation was consistent over many trials.

3 The Simulation Models

To ensure lack of errors and lack of sensitivity to model minutiae, we used two simulations developed independently by two coauthors (GS and TvO). We aimed for the simplest models that could reproduce the motion. Both of our models consist of two, 2D, rigid objects: a body and a leg. The body and leg are linked together by a two degree-of-freedom spring that also has damping. After a plastic (both in normal and tangential directions) collision with a rigid sloped ground, the foot, at the bottom of the leg, is assumed to have nonslipping contact, The two models only differ, in definition, in how the leaf spring constrains the relative motion between the leg and body.

Leaf spring: The spring, which on the physical device is a metal strip-spring (Fig. 1(*c*)), is initially modeled as an "Euler–Bernoulli" bending beam. It is clamped at each end and elastically resists relative rotation and translation (orthogonal to the spring) of the leg and body while allowing negligible motion along the spring. Although the simulations are fully nonlinear, the motions of the beam are considered to be those of linear beam theory.

We also allow some damping in the spring. The force and torque transmitted by the viscoelastic leaf-spring are approximated as linear in the relative linear and angular displacements and velocities. The axial (along the leaf spring) lack of extensibility is modeled as a constant-spring-length kinematic constraint. That is, we approximate the leaf-spring kinematics by constraining a point on the leg to move in a slot that is orthogonal to the leaf spring. According to these kinematics, an imagined point on a fictitious extension of the body, to near the leg end of the leaf spring, only moves on a line orthogonal to the leaf spring, as if in a slot in the body extension.

For one simulation, the slot is fixed in the body, on a rigid extension of the body, located at the leg end of the leaf spring (Fig. 2). The keyed slot elastically holds a point in the leg at a given position and the leg at a given angle.

The second simulation, otherwise identical in description, puts the slot on the leg instead of on the body.

Linearity demands that the transmitted force f_d and moment (torque) τ_θ can be written as

$$\begin{bmatrix} f_d \\ \tau_\theta \end{bmatrix} = C \begin{bmatrix} \dot{d} \\ \dot{\theta} \end{bmatrix} + K \begin{bmatrix} d \\ \theta \end{bmatrix} \tag{1}$$

The deformation variables d and θ are (respectively) the relative linear and angular displacements between the two objects. The 2×2 stiffness K and damping C are symmetric and positive semi-definite 2×2 matrices, as argued below.

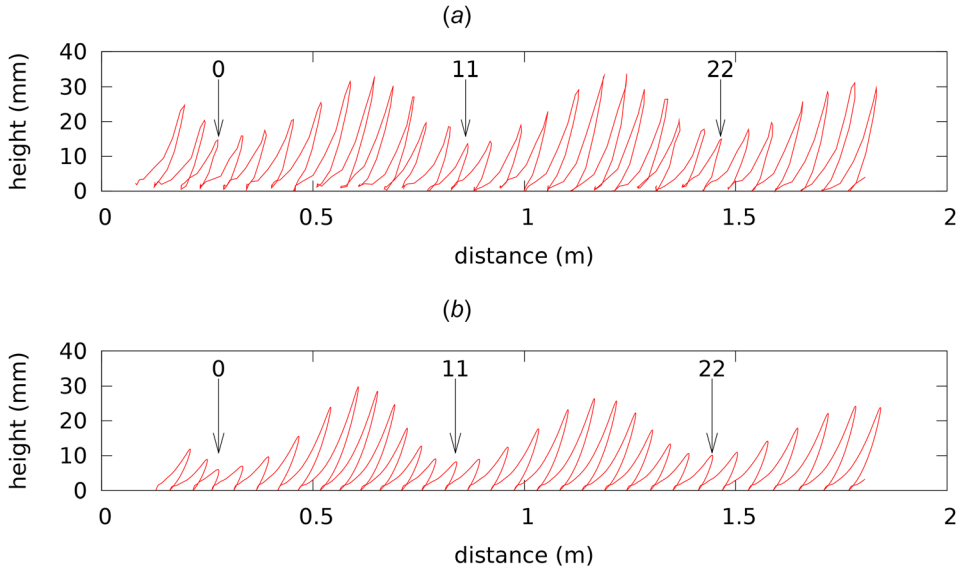

Fig. 6 Period ~11 oscillations. (*a*) In motion-capture data, the modulation of foot oscillations repeats approximately, but not exactly, every 11 hops. (*b*) As one might extrapolate from the argument of the totter eigenvalue (see text), the nonlinear simulation shows a variation in hopping amplitude that repeats about every 11 hops. (*a*) Motion capture—foot height versus distance hopped and (*b*) simulation—foot height versus distance hopped.

Stiffness: Classical Euler–Bernoulli beam theory yields that

$$K = -\frac{EI}{L}\begin{bmatrix} \frac{12}{L^2} & -\frac{6}{L} \\ -\frac{6}{L} & 4 \end{bmatrix} \quad \text{or} \quad K = \frac{EI}{L}\begin{bmatrix} \frac{12}{L^2} & -b\frac{6}{L} \\ -b\frac{6}{L} & 4 \end{bmatrix} \tag{2}$$

E is the material elastic modulus, I is the area moment of inertia of the spring cross section, L is the length of the beamlike leaf spring, and b is an extra off-diagonal parameter representing the coupling between rotation and translation in parameter studies ($b = 1$ for exact beam theory). The spring matrix K is positive definite so long as $b^2 < 4/3$. For this representation of the system, a conservative spring necessarily yields a symmetric K.

To first-order in spring displacements and rotations, the two simulation models are in principle identical. But, in our nonlinear simulations, these two linearizations of the spring have different nonlinear behavior.

Damping: The damping C must be positive definite to assure that it is dissipative. We reduce the parameter space by one variable using the common assumption of damping symmetry (Rayleigh dissipation function or the Onsager reciprocal relations [32]). We parameterize the damping matrix C in a way that assures that it will be symmetric and positive definite with three numbers c_1^2, c_2^2, and c_3 as follows:

$$C = R^{\mathrm{T}} C_{\mathrm{diag}} R \quad \text{where}$$
$$C_{\mathrm{diag}} = \begin{bmatrix} c_1^2 & 0 \\ 0 & c_2^2 \end{bmatrix} \quad \text{and} \quad R = \begin{bmatrix} \cos(c_3) & -\sin(c_3) \\ \sin(c_3) & \cos(c_3) \end{bmatrix} \tag{3}$$

The foot: The foot is modeled as a circular curve which rolls without slipping; the possibility of sliding contact was used in some trial simulations, but found to have a negligible effect (see Appendix B online under the "Supplemental Data" tab for this paper on the ASME Digital Collection). The ground collision is modeled as plastic (inelastic, dead, no bounce). At lift off, when the ground normal force goes to zero, the no-slip condition is released. This contact model is not necessarily self-consistent. But because, prior to foot release from sticking, there is a fortuitous forward slope of the leg at the same time that there is a retarding frictional force, we did not encounter, and thus did not have to contend with, the McGeer falling-pencil paradox [33].

In summary, the 2D model consists of a rigid object connected to a rigid leg by a two degree-of-freedom spring and damper, and the foot contacts the ground with no slip and no bounce.

3.1 Model Coordinates and Constraints. Assuming no-slip, we have four phases of motion: continuous flight, discontinuous collisional foot-strike, continuous stance, and lift-off. The lift-off phase involves a sudden change of governing equations, but involves no change of configuration nor velocity. In flight, we have three coordinates for each body (two center-of-mass position coordinates and a rotation angle (Fig. 2)). We also have one slot (inextensible leaf-spring) constraint. Flight thus has $3+3-1=5$ degrees-of-freedom. In stance, we have two additional constraints; the foot does not penetrate the ground and the foot rolls without slipping (Fig. 7(*a*)). This reduces the total degrees-of-freedom in stance to $5-2=3$.

3.1.1 Parameters. There are a total of 19 dimensional parameters in our mathematical model: 8 geometric and 11 mechanical.

Geometric: The eight geometric parameters describing the configuration in the robot's spring-relaxed state use coordinates referenced to a coordinate system located at the spring-relaxed hinge and oriented with the constraint slot. The lengths r_{0x}, r_{0y}, r_{1x}, and r_{1y} describe the x and y positions of the centers of mass of the body and leg; ℓ is the distance from the spring pivot point to the far edge of the foot measured along the line passing through both the pivot point and the center of the foot (total length is used instead of measuring to the foot center because this allows variation of total leg length and foot radius independently); α is the angle of the leg with respect to the body when the spring is relaxed; r_f is the radius of the round foot; and γ is the slope of the ramp.

Mechanical: The 11 mechanical parameters are m_0, I_0, m_1, I_1, the masses, and inertias about the COM for each object; g is the gravitational acceleration magnitude; K is the three-parameter spring matrix; and C is the three-parameter damping matrix.

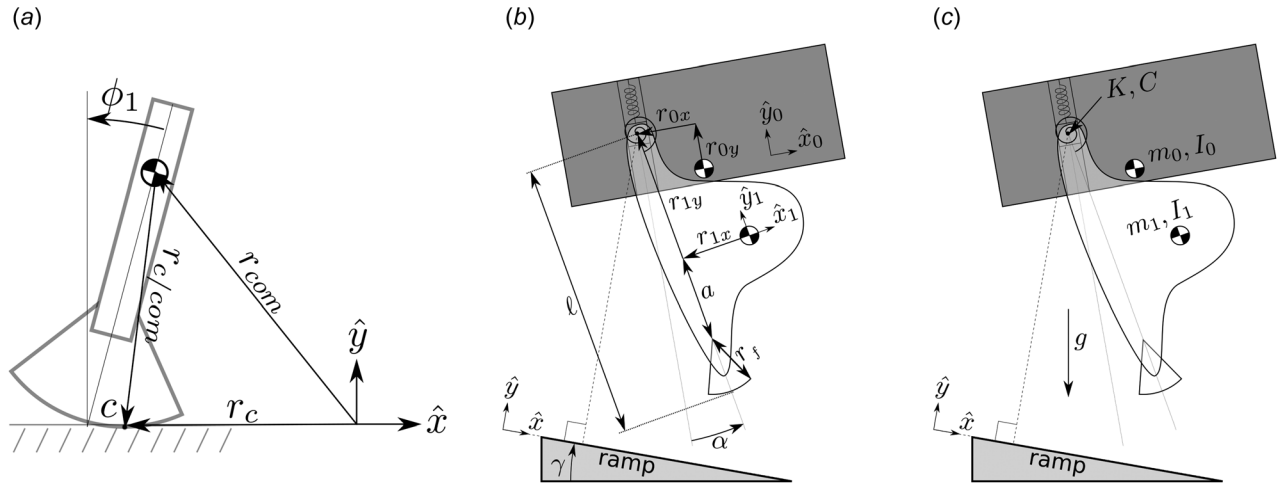

Fig. 7 (*a*) Nonslip rolling constraint. Rolling without slipping is enforced by the constraint $\dot{r}_c = 0$, where $r_c = r_{com} + r_{c/com}$. (*b*) Geometric parameters. There are eight geometric parameters, measured in the spring-relaxed configuration using a coordinate system at the hinge and oriented with the slot: two COM positions (4), foot position (2), foot radius (1), and ground slope (1); $4 + 2 + 1 + 1 = 8$. (*c*) Mechanical parameters. There are 11 mechanical parameters: masses (2), polar inertias (2), spring constants (3), damping constants (3), and gravity (1); $2 + 2 + 3 + 3 + 1 = 11$. See text and Appendix A online under the "Supplemental Data" tab for this paper on the ASME Digital Collection.

To reduce the number of independent parameters by three, we nondimensionalized all the parameters and dynamic variables, using the total leg length ℓ, the earth gravitational constant g, and body mass m_0 (Appendix A online under the "Supplemental Data" tab for this paper on the ASME Digital Collection).

3.2 System Identification (Parameter Estimation). Several parameters are easily measured with reasonable accuracy by taking the device apart: masses with a balance; centers of mass locations by hanging and knife-edge balance experiments; moments of inertia by swinging the parts as pendula and timing; leg lengths and angles with a ruler; and ground slope with digital level and a ruler (see Appendix C about slope variations under the "Supplemental Data" tab for this paper on the ASME Digital Collection).

The initial simulations used the spring matrix K from beam theory, based on the measured cross section and length of the leaf spring, and the elastic modulus of steel. The spring matrix K parameters were then refined using spring deflection experiments and by measuring vibration frequency of the leg when the body was clamped.

The damping parameters c_1, c_2, and c_3 were initially estimated by assuming decoupled modal damping in a leg vibration experiments. That is, we assumed the eigenvectors of C are the same as those of $M^{-1}K$ with M being the mass matrix of the leg with the body clamped. For example, we measured the characteristic decay time for the swing-dominant motion of the leg when supported by the spring attached to the clamped body. This was about 6.5 s corresponding to a dimensionless modal damping of $c_1 = 0.837$, with c_3 chosen to make the eigenvectors of C correspond to the eigenvectors of $M^{-1}K$.

Damping in the other, more-translational, mode is difficult to measure as it is hard to excite that mode in isolation. So, for initial simulations, we took $c_2 = 0$. The damping parameters were refined in further optimizations to better fit the hopping data, as discussed below.

The center-of-mass parameter r_{0x} is most directly affected by the single sliding-mass adjustment on the device (Fig. 2(*b*)). This position is physically adjusted often to improve performance. So, we consider r_{0x} as a free variable when fitting simulation to experiment.

For ground slope, we used a value close to that reported by Steinkamp and also used in our lab experiments, $\gamma \approx 0.079$. We varied the slope in the optimizations and also considered nonconstant slopes (discussed below).

4 Numerical Simulations

Given any standard formulation of Newtonian mechanics, the models described above are well posed. For both simulation models, we used a virtual power method [34] to obtain a system of differential algebraic equations (DAEs) which we solved by converting to systems of first-order ODEs (one set of equations for stance, one set for flight). In both models, the ODEs were integrated using an adaptive Runge–Kutta method (GS wrote his own custom method and TvO used Matlab's ODE45); constraint drift was corrected with constraint projection (GS) or constraint stabilization (TvO). Accurate numerical root-finding was used to detect the times of foot collision and foot release (Newton's method hand coded by GS and Matlab "events" by TvO). Jump-conditions for the velocity variables at foot-strike collision were found using angular momentum balance about the collision point. We estimate that typical numeric errors, relative to the exact mathematical model, are about 10^{-12} for each hop. For example, between collisions, with leaf-spring damping set to zero, energy is conserved to about 10^{-14}. As mentioned, as an added check, the equations of motion and numerical solutions were developed independently by two coauthors.

4.1 Periodic Motions. As for most analyses of passive-dynamic locomotion devices, we are concerned with the motions in the neighborhood of a periodic motion. The accurate finding of such a periodic motion, typically a limit cycle, is a numerical root-finding problem. That is, we seek initial positions and velocities, and an as-yet-unknown step period, so that numerical integration finds initial positions and velocities that are exactly recovered after a full cycle of motion (after one hop). There is no a priori guarantee that such a limit cycle exists, or, if it exists, that it can be found easily, or that it is unique. To find periodic motions (the root-finding problem), we seed our initial guess with a ballistic flight phase with duration that approximately matches the half-period of leg swinging in space (more exactly, half the period of the lowest mode of vibration of the leg swinging on a clamped body). Once a root is found, we characterize the stability of the periodic motion (limit cycle) using the eigenvalues of the linearization of the Poincaré map. The map we use is from the state just after foot collision to the state, found by numerical integration, just after the next foot collision. The Jacobian of this map

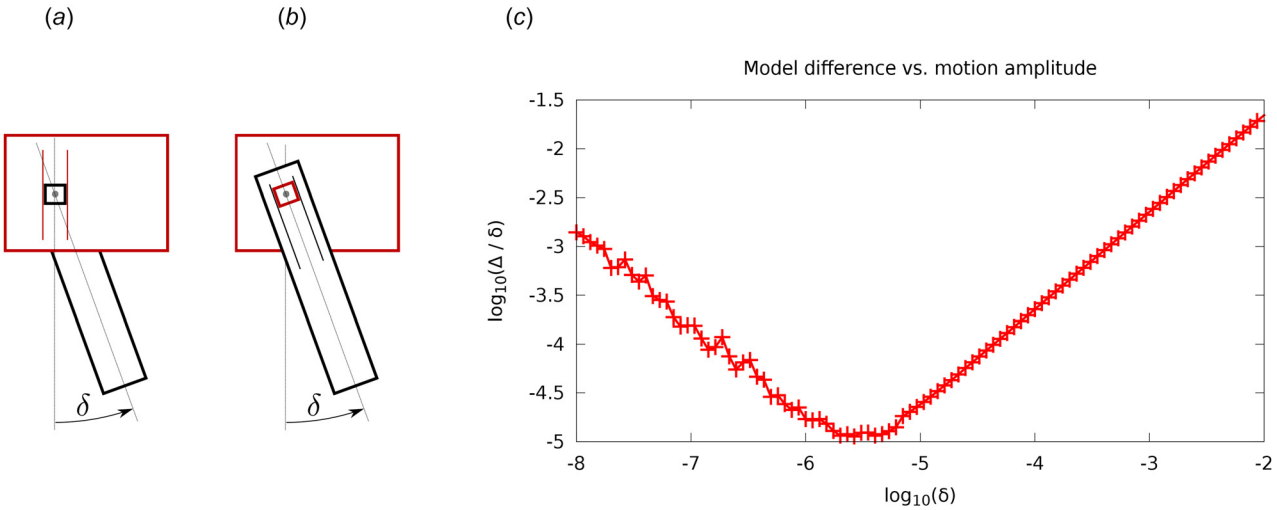

Fig. 8 Comparison of two models. (*a*) The model implemented by Stiesberg (GS), with the slot fixed in the body, and (*b*) the model implemented by van Oijen (TvO), with the slot fixed in the leg. (*c*) The difference between simulations of van Oijen and Stiesberg $\Delta(\delta) = |q_f^L - q_f^B|$, normalized by the magnitude δ of the initial state perturbation $\delta = |q_i - q^*|$, is shown as a function of perturbation magnitude δ. Linear convergence is seen as δ decreases to $\delta \approx 1\times10^{-5}$, at which point round-off error begins to dominate. Note that the minimum difference between the solutions $\Delta/\delta \approx 10^{-5}$, at $\log_{10}\delta \approx -5.5$, corresponds to an actual difference Δ of $\approx 1\times10^{-10}$ because of the normalization by δ; this normalization is also responsible for the slope ≈ -1 on the left of the graph which actually indicates a constant, not increasing, error with decreasing step size. For all of these calculations, an integration time step was chosen such that the errors above dominate the integration method errors.

is found by central difference calculation, based on perturbations of the initial state from the root (fixed point, limit cycle). The system is stable, neutrally stable (at least in the linearization), or unstable if the largest eigenvalue λ of the Jacobian of this map is less than, equal to, or greater than one in magnitude, respectively. In one of the two simulation sets (GS), the numerical method allows perturbations off of the Poincaré section and hence always has an irrelevant along-the-trajectory eigenvalue of zero.

For parameters close to those of the physical device, we always found at least one periodic motion (i.e., the root-finding always succeeded). Most often, two periodic motions were found for given system parameters: A long period solution close to the observed motions of the device and a short period solution. The short period solution for this hopper is similar to the short period solution in the Simplest Walker [35] in that it is always quite unstable and does not have leg retraction at heel strike. The long period solution has leg retraction at heel strike which perhaps contributes to the relative stability of that solution.

We generally ignored the short-period solutions. We also ignored solutions with multiple leg-swings in a single flight. We did not have to exclude flips (aerial somersaults) because our (relatively nonexploratory) root finder did not find flips.

Parameter refinement: Once periodic motions were found, we tuned the least-constrained-by-direct-measurement parameters, namely, the damping parameters c_2 and c_3. These two damping parameters were tuned so as to match the full device's period of hopping, step length, and a long-period eigenvalue (to be discussed) while minimizing the return-map Jacobian's largest eigenvalue.

In the initial simulations, we used video footage of the device provided by Steinkamp. We selected portions of video appearing to represent steady-state hopping motion (usually 10–20 hops after the hand-launch) to indirectly measure hopping frequency (total time divided by number of hops) and hop length (total distance divided by number of hops). The "Slow motion footage of final hopper" video on the supplemental data tab in Ref. [1] provided a particularly accurate measurement of hopping frequency. The corresponding hop length was easily calculated given a reference length (having Steinkamp measure the distance between points A and B on his ramp) and the hop count (between points A and B). Much later, we had motion-capture data that made accurate measurement of kinematic quantities easy and fortunately agreed with our initial measurements.

Several methods were used for parameter refinement, including manual "hand tweaking," human-guided line searches in a single parameter, systematic grid searches in discretized low-dimensional parameter neighborhoods, and optimizations in low-dimensional parameter neighborhoods. Matching observed hopping frequency and hop length was relatively easy by just varying the damping parameters c_2 and c_3 and mass position r_{0x}.

However, our attempt to simultaneously minimize the largest eigenvalue resulted in frustration as we expected to find stable hopping solutions but could not. Allowing many variations of parameters, as allowed by the inaccuracies of the system identification, we could not find a periodic motion with an eigenvalue inside the unit circle.

4.2 Two Independent Simulations. As described above, two independent models were implemented by coauthors GS and TvO; one considered the leg as sliding in a slot fixed in the body and the other with the body sliding in a slot fixed in the leg, respectively. The equations of motion for these two models were found separately as were the numerical simulations. In the limit of small motions near the spring's relaxed state, the states of the two models should differ only to first-order or higher in the spring-motion amplitude.

We checked agreement between our two simulations in free flight, at zero g. We started each model in a nonequilibrium state q_i perturbed from the spring-relaxed equilibrium q^*, integrated forward for 10 s (real time), then measured the difference between the final states for each model, q_f^L (slot in leg) and q_f^B (slot in body). With a perturbation size $\delta = |q_i - q^*|$, we expect the normalized final state difference $\Delta(\delta)/\delta = |q_f^L - q_f^B|/\delta$ to converge linearly as the perturbation size decreases. Figure 8 shows linear convergence of the normalized difference in state; in flight, our models and simulations are equivalent in the limit of infinitesimal motions.

As expected and hoped, even for the full nonlinear limit cycle calculations, the two models have close agreement. For example,

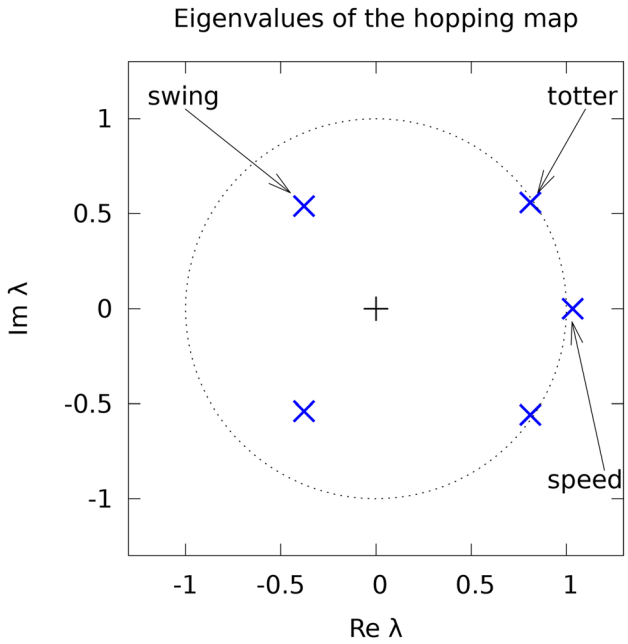

Fig. 9 Simulation eigenvalues. X's mark the complex eigenvalues on the complex plane. The unit circle is also shown. Parameters used are those that best fit the physical device and its motion. Only the speed eigenvalue is (barely) outside the unit circle; it is positive and real. The totter eigenvalues are slightly stable complex conjugate pair, and the swing eigenvalues are a quite stable (far inside the unit circle) complex conjugate pair.

with equal parameters, we find nearly equal eigenvalues of the return map. The qualitative and quantitative agreement between the two calculations enhances the credibility of both.

Finally, a simulation using a nonlinear ten-element model for the spring was compared to the simulations with the simple linearized spring; the difference between the nonlinear spring and linear spring simulations was about the same as the difference between the two independent simulations both with linear springs. Thus, the nonlinear spring model was not deemed worth the extra integration time for investigations of the hopper stability.

5 Comparison of Experiments With Simulations

Both of our two independent simulations reproduce all of these experimentally observed features:

- *Hopping the length of the ramp*. When launched at, or near the calculated periodic motion, the hopper hops the full length of the ramp. For initial conditions that differ slightly in the average forward speed from a periodic motion, the hop distance before a fall can be 4 m or more (the remaining length, after launch, of our experimental ramp), at least for a small appropriate range of launch speeds.
- *Kinematic details are matched*. Comparison of the foot motion and body–leg angle of the physical device and of the simulation is shown in Fig. 5.
- *Approximately period* ∼11 *motion is simulated*. Somewhat remarkably, if the simulated motion is started slightly off of the limit cycle, the (approximately) period ∼11 motion of the experiments is also reproduced (see Fig. 6(*b*)).

To achieve this matching (above), some of the poorly constrained parameters were allowed to be adjusted: the damping matrix parameters $c_1, c_2,$ and c_3 and the body COM position r_{0x}.

5.1 Stability Analysis. The physical device, started appropriately, hops the length of the ramp, seemingly stably. Our nonlinear simulations show hundreds of hops, if started on the (found from numerical root finding) limit cycle. So, we expected to more formally find stability in the simulations.

Stability of hopping map: As mentioned above, we numerically search for a fixed point of the five-dimensional Poincaré map, defined just after heelstrike, representing a periodic motion in the six-dimensional state space. This discrete hopping map is defined by the just-after-heel-strike Poincaré section. We find eigenvalues by numerical differentiation of the nonlinear simulation, using perturbation of the state near the fixed point. For our best match of the physical device's motion, the associated eigenvalues are shown in Fig. 9.

One of the eigenvalues is (slightly) outside of the unit circle, indicating that this model is unstable.

The magnitude of the unstable eigenvalue is about 1.03. As noted, both simulation models give similar values. The eigenvector corresponding to this unstable eigenvalue is dominated by the horizontal velocity variable so we call it the *speed mode*. McGeer's [24] passive running model also has a similar speed mode with an eigenvalue very close to 1. Related or not, we do not know, but conservative systems such as bicycles and tops always have a speed mode with an eigenvalue of *exactly* 1 (or zero, if treated as a continuous system) [36], corresponding to conservation of energy (in those conservative systems).

The totter mode: The eigenvalue labeled "totter" describes a fore-aft oscillatory pitch of the body (analyzed in the context of running by McGeer [24]). With $|\lambda_{\text{totter}}| = 0.985$, it is stable, but only slightly so.

However, whether growing or decaying in the experiments, the amplitude change is slow enough so that we are able to easily observe the slow oscillation of this mode in the real device. The eigenvalue of the totter mode has argument (phase angle) $\arg(\lambda_{\text{totter}}) = 0.558$. Thus, if the amplitude was exactly one, this would correspond to an oscillation with a period of about $2\pi/0.558 \approx 11$ iterations of the hopping map.

That is, the (approximately) period ∼11 oscillations visible in the motion-capture data (Fig. 6(*a*)) correspond to the totter mode of the linearized model. Note this is not a subharmonic, but a linear mode irrationally related to the fundamental hopping cycle.

We checked the dependence of the eigenvalues to a change in the body inertia. The biggest response to a change in body inertia is in the totter mode eigenvalue's argument (the phase). The totter amplitude (modulus) was relatively insensitive to body inertia. All other eigenvalues were also relatively insensitive to body inertia. Increasing body inertia causes a decrease in the totter mode argument. That is, increasing body inertia makes it so that more hops are in one complete totter cycle. This increased period of totter oscillations, which follows from increasing the body inertia, confirms the intuition that increased body inertia (i.e., the addition of the tail) resists fluctuations in body angle.

Some, but not all, motion-capture data sets show a slight decay with time of the amplitude of this mode, indicating that the magnitude of the totter eigenvalue may be slightly less than 1. An accurate experimental measurement of the magnitude of the totter eigenvalue (e.g., the growth or decay rate) using motion-capture data is not possible because of perturbations to the motion from bumps in the ramp (see Appendix C under the "Supplemental Data" tab for this paper on the ASME Digital Collection). The approximately period ∼11 totter is observed in all the datasets that have significantly variable hopping oscillations. (Thirty-seven data sets are long enough to detect variations of the period one motion. Twenty-three of these show systematic variation. In all of these 23, the period ∼11 totter mode is visible.)

5.2 Seeking Stable Periodic Orbits Using Parameter Optimization. Using our best estimates for the physical parameters, we get a good qualitative and quantitative match to the hopper motion but do not predict stable motions, the speed eigenvalue is always greater than 1 in magnitude. That is, the best-fit numerical models have slightly unstable hopping. Thus,

the observed ability of the hopper to hop the full ramp length must come from some combination of two effects:

(1) our model is slightly wrong and the physical device is actually slightly stable and/or
(2) the launches of the physical device are accurate enough so that multiplying initial errors by $\lambda^{100} \approx 1.03^{100} \approx e^3 \approx 20$ does not knock the hopper down.

We accept, as possible but unlikely, a third possibility that the physical system has a stable nonlinear attractor. We think this is unlikely because our nonlinear simulations, no matter how accurately started, always lead to falls after ≈700 steps. That is, in the nonlinear simulations falling occurs about when it would be expected from a linear calculation started with a 10^{-10} accuracy ($\lambda^n \times \varepsilon \approx 1.03^{700} \times 10^{-13} \approx 0.1$). No indefinitely long hopping was numerically found with physically motivated parameters nor with parameters sought in optimizations of stability (see below). Meanwhile, the numerical simulations show signs of being indicative of true behavior by its correct prediction of overall motion, including the subtle effect of period ∼11 motion. From the physical data we have we cannot, however, exclude that unmodeled, or poorly modeled, effects cause the existence, on the physical model, of something that would be described as a stable attractor. The evidence we have suggests that the physical device does not have a stable attractor and the latter parts of this paper rest on this not-fully proven property.

Attempts to make the simulation model stable, using parameters close to the physical device, using intuitive hand tuning and simple line searches, all failed. Corralling one eigenvalue into the unit circle inevitably scares another one out. So, we attempted more systematic eigenvalue optimization using the GS model: minimize the largest eigenvalue magnitude while varying the parameters within a bounded neighborhood representing the maximum uncertainty in the device properties. As noted, the parameters with greatest uncertainty are those related to the damping matrix and horizontal COM position of the body. A random descent optimization method was used that attempts to track a periodic root while doing a random walk in parameter space; random steps that do not decrease the objective function are rejected.

Starting with a periodic motion, the algorithm iterates the following sequence:

- calculate the derivative of the objective function dF/dP, where F is the scalar objective function and P is the vector of model parameters to vary,
- change to a new parameter vector $P_{n+1} = P_n + \delta P$, where δP is a perturbation in a random direction normalized to satisfy $\delta F \times dF/dP = \delta F$, where δF is the desired change in objective function per optimization step,
- find the new periodic root, if possible; it is important that a sufficiently small δF is chosen so that a new root can be found, and
- if the new periodic root is found and decreases F, then keep P_{n+1}, else restore the previous parameter set, $P_{n+1} = P_n$.

The objective function F was chosen to be the maximum eigenvalue magnitude. The derivative dF/dP was evaluated less frequently, every 20 iterations or so, to save computational effort. The maximum magnitude of δF is limited by the ability of the root-finding algorithm to converge on the new root, if it exists. In the case of an approach to a smooth local minimum, each element of dF/dP will vanish, so trying to scale δP to satisfy $\delta P \times dF/dP = \delta F$ will cause δP to grow without bound. Therefore, to avoid the algorithm failing to converge in precisely the areas of parameter space we are trying to find, the maximum size of δP is limited. However, our largest eigenvalue magnitude is, in general, a nonsmooth function of the parameters. The example in Fig. 10 is typical of our optimization runs in that, in the neighborhood of a minimum of the maximum eigenvalue, the magnitude of the maximum is a continuous but nondifferentiable function of

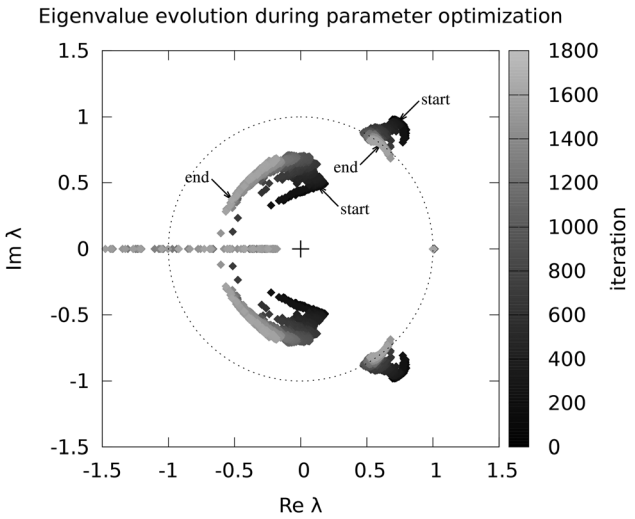

Fig. 10 Optimization of maximum simulation eigenvalue. The eigenvalues corresponding to the initial parameter set and the last accepted parameter set are marked by arrows labeled "start" and "end," respectively. The initial parameter set was intentionally chosen to destabilize the totter modes. The optimization succeeds in stabilizing the totter modes, but not the speed mode, which remains very close to $\lambda = 1$ for the entire optimization run. All the iterations in this optimization run are shown: the successes that reduce the maximum eigenvalue and the failures that sometimes drastically increase the maximum eigenvalue. The problem is that the eigenvalues for the swing eigenmodes become real, with one of them growing quickly along the negative real axis and thus obviating reduction of the speed mode eigenvalues.

the parameters. Individual eigenvalues are smooth functions of the parameters, except when two real roots coalesce into a complex pair (or the reverse). However, when one mode takes over from the other as maximum, the magnitude of the maximum is not smooth (the max of two smooth real functions is nonsmooth where the two functions cross). One of these two nonsmoothnesses is the common case at a local minimum of the maximum eigenvalue.

This optimization loop is repeatedly run and repeatedly fails to decrease the objective function $n = 200$ consecutive times before quitting; the resulting best value was assumed to be an approximation of a local minimum. Restarting the optimization with the candidate local minimum (above) always terminates with very little or no change to the parameter set. This method explores more parameter space than a typical gradient method; two runs with identical (not already optimized) initial parameter sets will, with high probability, take different paths in parameter space.

We did some exploration of the space of initial periodic seeds for the optimizations above. As noted previously, for a given parameter set there is often another period-1 solution, but it is highly unstable with no leg back-swing just before impact. Other more exotic unstable solutions that involved multiple leg swings were found, but no other almost-stable period-1 or period-2 solutions.

5.3 Broader Parameter Searches. Is the lack of stable solutions somehow fundamental, or just a result of the region of parameter space in which we were searching? Note, as mentioned in the introduction, others have found simulations of passive running that are stable. To address this question for this model, we broadened the parameter search, using eigenvalue optimizations that had initial seeds with parameters far from the physical device. Far from the actual hopper design, we have found motions that are stable according to limit-cycle stability analysis. These parameter

sets are notably different than the Steinkamp hopper, having, for example, a large round foot and a heavy leg.

Relaxing the search for stable motions still further, to include period-2 motions, we found stable period-2 motions with a maximum eigenvalue as low as 0.81 accompanied, however, with an unstable period-1 motion. There are significant differences in this parameter set (shown in Fig. 15), such as a much heavier leg and smaller body moment-of-inertia.

Key, however, is that in the neighborhood of the actual (apparently stable) device, we could not find stable simulations. That is, all of our attempts to follow any motion, stable or unstable, starting in the neighborhood of the device's physical parameters, and then continuously deforming the parameter set to other neighborhoods, failed. Solutions simply disappear. The reverse procedure, trying to follow a known stable solution (using the techniques described above in the random descent optimization method) in a non-Steinkamp-like parameter neighborhood, while moving, on average, toward the parameters of the device, also fails.

The useful search space is rather restricted by two effects. First, for the parameters we chose, the parameter neighborhood that is plausibly like the actual Steinkamp hopper looks, perhaps, something like a squashed ellipsoid—some directions (in this parametrization) are tightly bound because we have accurate measurements of those parameters, other directions are relatively free, corresponding to uncertainty in those parameters. On the other hand, some search directions show an extreme sensitivity to parameter values, with the largest eigenvalue growing rapidly with deviations in those directions. Combining these effects, the search region, as we have parametrized it, seems (in our informal probes) to be quite restricted. This claim is only based on our investigations, not on any systematic parameter space characterization.

However, we cannot claim that our search is exhaustive, only that we tried hard.

6 Results of Simulation Optimizations

At this point, the situation is this:

(1) Steinkamp's physical hopper seems stable in that it can hop 100^{+} times without falling.
(2) Our two simulations, using measured parameters of the physical device, both match various features of the physical device, including foot trajectory, frequency of hop, body angle versus time, and the existence of an approximately period ~11 motion.
(3) All the simulations that reasonably match device parameters are unstable, with a largest eigenvalue equal to at least 1.002, and typically 1.03.
(4) The nonlinear simulations show no sign of a more complex attractor.

An apparent contradiction: We have an apparent contradiction. After 100 hops, an initial perturbation, a deviation from a perfect limit-cycle launch, should grow by about a factor of $1.03^{100} \approx (1.03^{33})^3 \approx e^3 \approx 20$. How could people launch the device accurately enough so that this 20× amplification would not lead to falling?

6.1 The Importance of Launching Technique. As noted, when Steinkamp, or another practiced person, launches the device, they gently hold the back of the body for the first 10–15 hops (see Fig. 4), while simultaneously walking along with it. Perhaps a practiced launcher finds, or nearly finds, the limit cycle motion?

Simulating launch: We made a simulation model of this launch: the fingers gently holding the tail in motion are modeled as a spring and parallel damper connected between a point on the tail and a rigid constant-velocity point, modeling the wrist. In detail (see Fig. 4(*b*)):

- The spring and damper are connected in a parallel configuration like a shock absorber.
- One end of the shock absorber is connected to a point (x_m, y_m) fixed on the tail.
- The other end of the shock absorber is connected to a moving reference point with a prescribed constant-velocity x coordinate and y coordinate equal to that of the fixed point on the tail (equivalent to a ring sliding up and down on a vertical pole that is the y axis of the coordinate system containing the moving reference point).

So, the spring and damper act only on the horizontal separation and horizontal speed difference between the hand and a point on the device tail

$$\mathbf{f}_l = [k_l(x_m - v_l t) + c_l(\dot{x}_m - v_l)]\hat{x} \tag{4}$$

This implicitly defines the x coordinate of the reference point ($v_l t$) as zero at time $t = 0$.

For a broad range of spring and damping constants, this *supported* hopping system is stable, with a maximum eigenvalue as low as 0.8. The maximum eigenvalue magnitude of the held-launch hopping map at its fixed point, as a function of spring and damping, is shown in Fig. 11.

This stable fixed point is not, however, the same as for the free-hopper, even for the same forward speed. So, using this launch model, at the instant the launcher is disconnected, we can interpret the state of the free hopper as that of the free hopping fixed point plus a perturbation (in the full state) corresponding to the difference between the held fixed point and the free fixed point. After release, the perturbation grows with each hop until the hopper falls over. According to simulation, the distance hopped with such a launch varies with the launch speed as shown in Fig. 12; a hopping distance greater than 4 m is predicted by simulations for a range of launch speeds $0.544 < v_l < 0.609$. The predicted size of this launch-speed interval is only slightly affected by including nonflatness of the ramp (see Appendix C under the "Supplemental Data" tab for this paper on the ASME Digital Collection).

The average force applied to the hopper by the launching device (spring and damper) is shown in Fig. 12. Note that the holding force is smooth, monotonically decreasing and changes

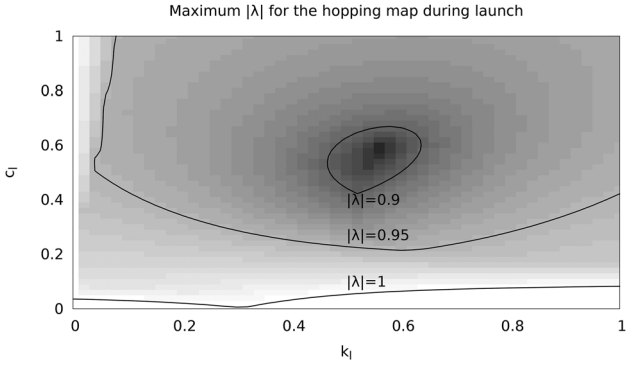

Fig. 11 Maximum eigenvalue during simulated launch. The maximum eigenvalue magnitude for the periodic motion of the held hopper (the modeled launch condition) is shown as a function of spring and damping parameters k_l, c_l, with a constant launch speed $v_l \approx 0.551$, equal to the free hopping map fixed point speed. This launch map has a stable fixed point over the majority of the parameter space shown. The boundary of stability, the $|\lambda| = 1$ contour, overlaps the interval of the vertical axis shown here for $c_l > \approx 0.03$; on this interval, numerics and reasoning agree that the maximum eigenvalue approaches exactly 1 as k_l approaches 0 (see text). The coordinate of the attachment point in the body-fixed coordinates (see Fig. 4(*b*)) is $(x_m, y_m) = (-0.8, 1.0) * \ell$. The stability depends on the attachment coordinate y_m; with too low a grip, the sliding ring contact does not adequately couple to the totter mode. With too high a grip, the dashpot does not adequately couple to the hopper's speed mode.

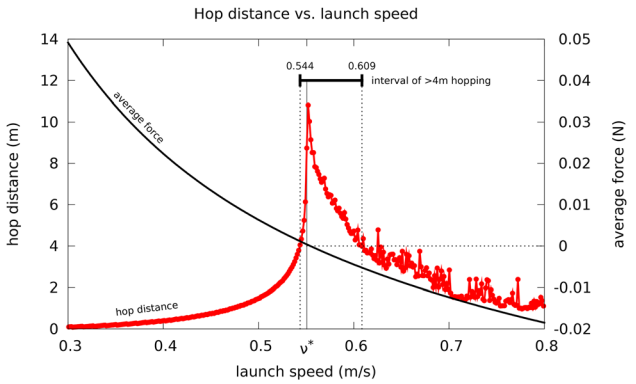

Fig. 12 Hopping distance as a function of launch speed. The hopper is launched from a stable periodic state of the shock-absorber held system. For each different speed, there is a different perturbation from the free periodic motion. Using this launch model, simulations predict a hopping distance greater than 4 m for a range of launch speeds $0.544 < v_l < 0.609$; the magnitude of this interval is 0.065, somewhat but not substantially larger than the interval for a simulation with a bumpy slope (compared to Fig. 17(*b*) in Appendix C under the "Supplemental Data" tab for this paper on the ASME Digital Collection). The spring and damping coefficients are $k_l = 0.5$ and $c_l = 0.5$. The fixed point of the free hopping map has a speed $v^* \approx 0.551$. Note that even launching at the free-hopper limit-cycle speed, the distance to falling is not infinite because the held hopper has a different fixed point than the free hopper. Launch force as function of launch speed. The average launching force is a smooth monotonically decreasing function of the launch speed and crosses zero near the unstable free hopping map fixed point speed v^*. The average forces exerted on the device during this type of launch are similar to that of a penny resting on your finger, about 0.03 N. For launch speeds less than v^*, the instability would cause the robot to decelerate. Therefore, a positive force is needed to maintain constant speed. Conversely, at launch speeds greater than v^*, the instability would cause the robot to accelerate; therefore, a negative force is needed.

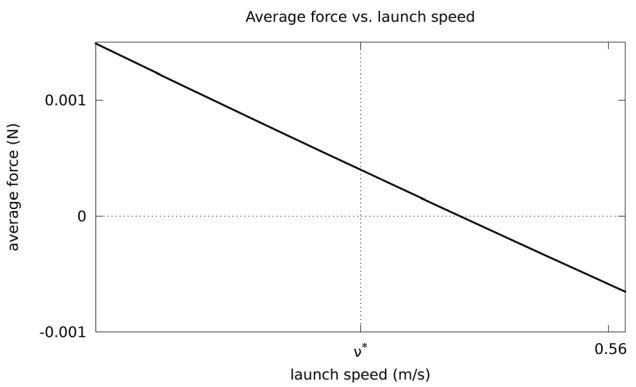

Fig. 13 Launch force as a function of launch speed—a closer look. A magnified view of the force shows that it does not vanish at the free limit cycle speed v^*. This is consistent with the fact that the limit cycle at launch is not the same as the free limit cycle and indeed never can be the same for this launch technique.

sign very near the optimal launching speed. This implies a simple strategy for learning the right launch speed: force minimization. However, as shown in Fig. 13, the force does not vanish at the free limit cycle speed.

Our hypothesis is that a practiced launcher has learned to launch roughly as follows:

- Hold onto the tail loosely while slowly varying the near-constant hand speed;
- Find the speed which minimizes the force felt in the fingers;
- When the force is minimized, let go; and
- If the robot falls back, change the speed so that the robot leans more forward at the next launch; if it falls forward, change the speed to make a more backward force.

No matter the spring or damping constant, we cannot find a stable held-hopping that has exactly the free-hopper's limit cycle. So, this launch technique, while possibly good enough, is intrinsically imperfect.

Summarizing the launch-model features:

- The simulated launch stabilizes the device while held during launch (for appropriately chosen stabilizing spring and damping coefficients as shown in Fig. 11).
- A good launch speed, one that leads to initial conditions close to the periodic motion, is easy to find by using a simple, intuitive force feedback strategy: adjust the speed to minimize the force applied.

Stability versus not-so-bad instability: A functional robotic device or any animal will use a control system, at least to steer and navigate. Typically for animals at the human scale or smaller this happens with a time scale on the order of 1 s, shorter than the characteristic instability time of this robot ($\lambda \approx 1.03$, step period $\approx 0.09\text{s} \Rightarrow$ characteristic time $\approx 0.09\text{s}/\ln(1.03) \approx 3\text{s}$). Given that corrections are made for other purposes, more often than the instability time, there is no practical difference between a technically unstable passive eigenvalue magnitude of $\lambda_{\max} = 1.03$ and, say, a technically stable $\lambda_{\max} = 0.97$.

7 Conclusions

Given the superficially stable motions of Steinkamp's physical hopper, the results of our investigations were unexpected. We assumed that we could make a simple simulation model that would fit the observed motions and for which we would calculate stability. We expected to find hopping results analogous to the discoveries made for walking in the study of the simplest walking model [2,37]. Further, we already knew that at least according to one theory [24], passive stable running was possible in 2D.

But truth seems to differ from our previous expectations: we could not find stable solutions for our models of the Steinkamp hopper. Rather, we found a hopping motion that is just barely *unstable*. Model parameters that lead to prediction of stability were not close to those that well-modeled the physical device. On the other hand, we found a model for the human launcher that explains how the device might be launched so close to its unstable limit cycle that falling consistently does not occur within 100 hops, although we predict that eventual falling is inevitable.

The broader message is that, for systems which are to be used only for finite time T, or which are controlled with a characteristic time T, whether a system is technically stable or instead is technically unstable but with a characteristic time longer than T is of no practical import. For such dynamical systems, the key distinction is not stability versus instability but whether the characteristic time for a perturbation to grow by a factor of, say, e is less than or greater than a typical control or operation time T (with the latter case being functionally equivalent to passive stability).

Acknowledgment

Thanks to Peter Steinkamp for his discussions and help with data collection and editing. Thanks to Tim Richardson of Fast Video NW, Vancouver, WA for high-speed video footage. Thanks to Pranav Bhounsule for the B&W portion of the strobe motion figure and for useful discussions. Thanks to Michael Coleman for the Working Model simulation that motivated the stable period-2 hopping model. Thanks to Scott Bollt and Matt Sheen for their help in editing. We used an NSF IGERT funded Vicon IR camera

system. This research was facilitated by NSF Grant Nos. E558433, E808388, and E558393.

Nomenclature

$C = 2 \times 2$ damping matrix
$c_l =$ dampinglike parameter for the simulated launch model
$d =$ relative linear displacement between body and leg
$F =$ scalar objective function to be minimized while seeking an optimum parameter set
$f_d =$ force between body and leg dependent on relative linear displacement δ
$f_l =$ force applied on the hopping model during a simulated launch
$K = 2 \times 2$ stiffness matrix
$k_l =$ springlike parameter for the simulated launch model
$M =$ mass matrix of the leg when the body is clamped
$P =$ vector of model parameters used for an optimization run
$q_f =$ final state vector of hopper
$q_i =$ initial state vector of hopper
$t_\theta =$ torque between body and leg dependent on relative angular displacement θ
$v_l =$ speed of the moving reference frame for the simulated launch model
$x_m = x$ coordinate of the shock attachment point for the simulated launch model
$y_m = y$ coordinate of the shock attachment point for the simulated launch model
$\delta =$ magnitude of perturbation to initial state vector of hopper
$\theta =$ relative angular displacement between body and leg
$\lambda =$ eigenvalue of linearized hopping map
$v^* =$ forward speed of the hopping model at the periodic limit cycle

References

[1] Steinkamp, P., 2017, "A Statically-Unstable Passive Hopper: Design Evolution," ASME J. Mech. Rob., **9**(1), p. 011012.
[2] Coleman, M., and Ruina, A., 1998, "An Uncontrolled Walking Toy That Cannot Stand Still," Phys. Rev. Lett., **80**(16), pp. 3658–3661.
[3] Kooijman, J., Meijaard, J., Papadopoulos, J. M., Ruina, A., and Schwab, A., 2011, "A Bicycle Can Be Self-Stable Without Gyroscopic or Caster Effects," Science, **332**(6027), pp. 339–342.
[4] Hubbard, M., 1979, "Lateral Dynamics and Stability of the Skateboard," ASME J. Appl. Mech., **46**(4), pp. 931–936.
[5] Ruina, A., 1998, "Nonholonomic Stability Aspects of Piecewise Holonomic Systems," Rep. Math. Phys., **42**(1), pp. 91–100.
[6] Raibert, M., and Tello, E., 1986, "Legged Robots That Balance," IEEE Expert, **1**(4), p. 89.
[7] Raibert, M., Brown, H., and Chepponis, M., 1984, "Experiments in Balance With a 3d One-Legged Hopping Machine," Int. J. Rob. Res., **3**(2), pp. 75–92.
[8] McGeer, T., 1990, "Passive Dynamic Walking," Int. J. Rob. Res., **9**(2), pp. 62–82.
[9] Garcia, M., Chatterjee, A., and Ruina, A., 2000, "Efficiency, Speed, and Scaling of Two-Dimensional Passive-Dynamic Walking," Dyn. Stab. Syst., **15**(2), pp. 75–99.
[10] Cham, J., and Cutkosky, M., 2007, "Dynamic Stability of Open-Loop Hopping," ASME J. Dyn. Syst. Meas. Control, **129**(3), pp. 275–284.
[11] Dankowicz, H., and Piiroinen, P., 2002, "Exploiting Discontinuities for Stabilization of Recurrent Motions," Dyn. Syst. Int. J., **17**(4), pp. 317–342.
[12] Reddy, C., and Pratap, R., 2000, "Can a Passive Hopper Hop Forever?" Curr. Sci., **79**(5), pp. 639–645.
[13] Seth, B., Seshu, P., Shanmuganathan, P., Vichare, V., and Raj, P., 2007, "Search for Initial Conditions for Sustained Hopping of Passive Springy-Leg Offset-Mass Hopping Robot," ASME J. Dyn. Syst. Meas. Control, **129**(4), pp. 522–526.
[14] Owaki, D., Koyama, M., Yamaguchi, S., Kubo, S., and Ishiguro, A., 2010, "A Two-Dimensional Passive Dynamic Running Biped With Knees," IEEE International Conference on Robotics and Automation (ICRA), Anchorage, AK, May 3–8, pp. 5237–5242.
[15] Ahmadi, M., and Buehler, M., 1997, "Stable Control of a Simulated One-Legged Running Robot With Hip and Leg Compliance," IEEE Trans. Rob. Autom., **13**(1), pp. 96–104.
[16] Sayyad, A., Seth, B., and Issac, K., 2007, "Dynamics and Control of a One-Legged 2-D SLOM Hopping Robot," 12th IFToMM World Congress, Besancon, France, June 18–21.
[17] Geyer, H., Seyfarth, A., and Blickhan, R., 2006, "Compliant Leg Behaviour Explains Basic Dynamics of Walking and Running," Proc. R. Soc. B, **273**(1603), pp. 2861–2867.
[18] Ghigliazza, R., Altendorfer, R., Holmes, P., and Koditschek, D., 2003, "A Simply Stabilized Running Model," SIAM J. Appl. Dyn. Syst., **2**(2), pp. 187–218.
[19] Owaki, D., and Ishiguro, A., 2007, "Mechanical Dynamics That Enables Stable Passive Dynamic Bipedal Running-Enhancing Self-Stability by Exploiting Nonlinearity in the Leg Elasticity," J. Rob. Mechatronics, **19**(4), pp. 374–380.
[20] M'Closkey, R., and Burdick, J., 2002, "An Analytical Study of Simple Hopping Robots With Vertical and Forward Motion," 1991 IEEE International Conference on Robotics and Automation (ICRA-02), Sacramento, CA, Apr. 9–11, pp. 1392–1397.
[21] Hyon, S.-H., and Emura, T., 2002, "Quasi-Periodic Gaits of Passive One-Legged Hopper," IEEE/RSJ International Conference on Intelligent Robots and Systems (IRDS), Lausanne, Switzerland,, Sept. 30–Oct. 4, Vol. 3, IEEE, pp. 2625–2630.
[22] Zeglin, G., and Brown, B., 1998, "Control of a Bow Leg Hopping Robot," IEEE International Conference on Robotics and Automation (ICRA), Leuven, Belgium, May 16–20, Vol. 1, pp. 793–798.
[23] Brown, B., and Zeglin, G., 1998, "The Bow Leg Hopping Robot," 1998 IEEE International Conference on Robotics and Automation (ICRA), Leuven, Belgium, May 16–20, Vol. 1, pp. 781–786.
[24] McGeer, T., 1990, "Passive Bipedal Running," Proc. R. Soc. London, Ser. B, **240**(1297), pp. 107–134.
[25] Cotton, S., Olaru, I. M. C., Bellman, M., van der Ven, T., Godowski, J., and Pratt, J., 2012, "FastRunner: A Fast, Efficient and Robust Bipedal Robot. Concept and Planar Simulation," IEEE International Conference on Robotics and Automation (ICRA), St. Paul, MN, May 14–18, pp. 2358–2364.
[26] Mombaur, K., Longman, R., Bock, H., and Schlöder, J., 2005, "Open-Loop Stable Running," Robotica, **23**(1), pp. 21–33.
[27] Owaki, D., Osuka, K., and Ishiguro, A., 2013, "Stabilization Mechanism Underlying Passive Dynamic Running," Adv. Rob., **27**(18), pp. 1399–1407.
[28] Paul, C., Dravid, R., and Iida, F., 2002, "Control of Lateral Bounding for a Pendulum Driven Hopping Robot," 5th International Conference on Climbing and Waffling Robots (CLAWAR 2002), Paris, France, Sept. 25–27, pp. 333–340.
[29] Steinkamp, P., 2015, "Unpowered Walkers and Hoppers," Portland, OR, accessed Mar. 14, 2015, http://www.hevanet.com/psmfg/web%20site/passive.html
[30] Seyfarth, A., Geyer, H., and Herr, H., 2003, "Swing-Leg Retraction: A Simple Control Model for Stable Running," J. Exp. Biol., **206**(15), pp. 2547–2555.
[31] Hasaneini, S. J., Macnab, C. J., Bertram, J. E., and Leung, H., 2014, "Swing-Leg Retraction Efficiency in Bipedal Walking," IEEE/RSJ International Conference on Intelligent Robots and Systems (IROS 2014), Chicago, IL, Sept. 14–18, pp. 2515–2522.
[32] Pathria, R. K., 1996, *Statistical Mechanics*, 2nd ed., Butterworth Heinemann, Oxford, UK.
[33] McGeer, T., and Palmer, L. H., 1989, "Wobbling, Toppling, and Forces of Contact," Am. J. Phys., **57**(12), pp. 1089–1098.
[34] Schwab, A. L., 1998, *Multibody Dynamics B*, Delft University of Technology, Delft, The Netherlands.
[35] Garcia, M., Chatterjee, A., Ruina, A., and Coleman, M., 1998, "The Simplest Walking Model: Stability, Complexity, and Scaling," ASME J. Biomech. Eng., **120**(2), pp. 281–288.
[36] Meijaard, J., Papadopoulos, J., Ruina, A., and Schwab, A., 2007, "Linearized Dynamics Equations for the Balance and Steer of a Bicycle: A Benchmark and Review," Proc. R. Soc. A, **463**(2084), p. 1955.
[37] Coleman, M. J., Garcia, M., Mombaur, K., and Ruina, A., 2001, "Prediction of Stable Walking for a Toy That Cannot Stand," Phys. Rev. E, **64**(2), p. 022901.
[38] Baraff, D., 1993, "Non-Penetrating Rigid Body Simulation," 14th European Association for Computer Graphics Conference (Eurographics 93), Barcelona, Spain, Sept. 6–10.